Pergamon

Adv. Space Res. Vol. 20, No. 4/5, pp. 683–693, 1997

Printed in Great Britain
0273-1177/97 $17.00 + 0.00

PII: S0273-1177(97)00456-0

PLASMA WAVES IN THE UPSTREAM AND BOW SHOCK REGIONS OBSERVED BY GEOTAIL

H. Matsumoto*, H. Kojima*, Y. Kasaba*, T. Miyake*, R. R. Anderson** and T. Mukai***

**Radio Atmospheric Science Center, Kyoto University, Uji, Kyoto 611, Japan*
***Department of Physics and Astronomy, The University of Iowa, Iowa City IA 52242-1479, U.S.A.*
****Institute of Space and Astronautical Science, Sagamihara, Kanagawa 229, Japan*

ABSTRACT

Upstream waves in the foreshock of the Earth's bow shock are the manifestation of microscopic plasma dynamics caused by the solar wind interaction with the bow shock. Though the past wave observation has revealed many interesting features of the foreshock plasma waves, the lack of waveform observation could not provide sufficient information to understand the micro-physics of wave-particle interactions beyond certain points. The present paper describes the preliminary results of the GEOTAIL plasma wave observation in the upstream as well as in the bow shock regions. The waveform capture (WFC) receiver has revealed interesting waveforms in these regions which are to provide a clue of understanding the micro-physics involved in the wave generation in the upstream and bow shocks. Based on the observed information, we classify the electron and ion foreshock regions into more detailed structures. We also have carried out some simple computer simulations to understand some of the observed wave phenomena.

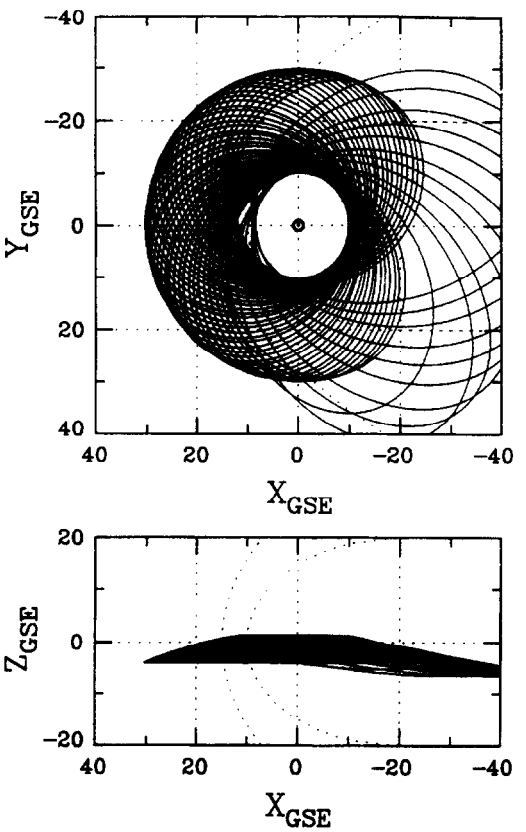

Fig. 1 Near Earth orbits of GEOTAIL for a period of Nov., 1994 - Nov., 1995.

INTRODUCTION

In November of 1994, GEOTAIL was transferred into the near Earth orbits from its distant tail orbits. Since then it has crossed the bow shock frequently on a regular basis. Figure 1 shows the orbits of GEOTAIL after being transferred into the near Earth orbit for a period from November, 1994 to November, 1995. Before the orbit transfer to the near Earth orbits, GEOTAIL had surveyed the distant tail region. Figure 2 shows a schematic illustration of the plasma waves which have been detected in the different regions in the tail and the dayside magnetosphere by the

GEOTAIL Plasma Wave Instrument (PWI). All wave modes observed by GEOTAIL, as illustrated in the figure, had been observed by previous spacecraft such as OGO series, IMP series and ISEE satellites (e.g., see Gurnett, 1985 and references therein). However there are two points in which the GEOTAIL PWI added new information to the previous knowledge on plasma waves in the near Earth space.

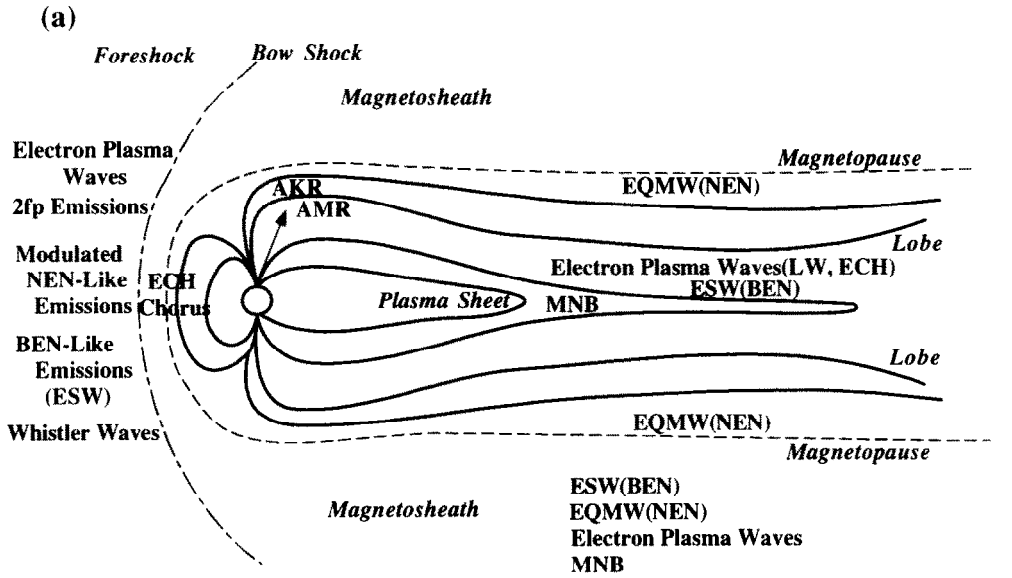

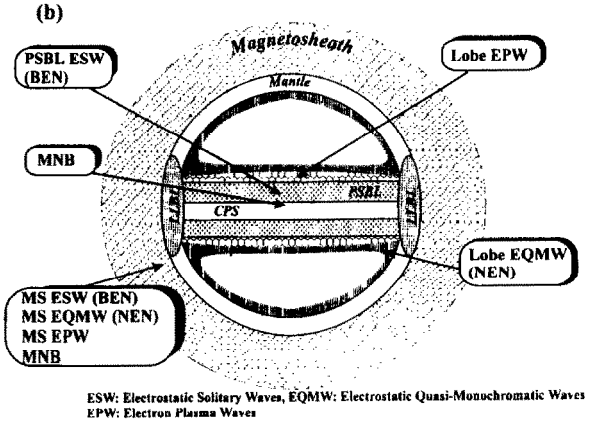

Fig. 2 Schematic illustration of plasma waves detected by GEOTAIL/PWI in geospace. (a) Meridian cut; (b) Tail cross section.

One comes from the advantage of the GEOTAIL orbits. The GEOTAIL area coverage in the magnetotail is much broader than any past spacecraft's. Therefore we could collect more detailed information of plasma waves over much broader regions with more frequent observations. This makes it possible for a statistical study. One example of such is an attempt of studying the global structure of the magnetotail based on the different wave signatures at different regions (Kojima *et al.*, 1997).

Second new information collected by the PWI is on waveform or wave phase which had not well been disclosed. Most of the previous studies on plasma waves have been based mainly on the spectral observation by sweep frequency analyzer (SFA) with high frequency resolutions and multi-channel analyzers (MCA) with high time resolutions. The GEOTAIL PWI is equipped with a waveform capture (WFC) receiver in addition to the conventional SFA and MCA (Matsumoto *et al.*, 1994a). The WFC can capture waveforms of two electric components and three magnetic components simultaneously for 8.7 seconds in every 5 minutes. The maximum frequency covered by the WFC is 4 kHz. One example of such new findings based on the WFC is disclosure of a new aspect of the wave features of the broadband electrostatic noise (BEN). The WFC has revealed that the BEN (or at least the high frequency part of the BEN) is composed of a series of isolated (solitary) bi-polar electric pulses which is named as Electrostatic Solitary Waves (ESW). The nature of the solitary pulses for BEN was first recognized by the waveform observation in time domain (Matsumoto *et al.*, 1994b; Kojima *et al.*, 1994). The past observation of BEN had been made only in frequency domain by

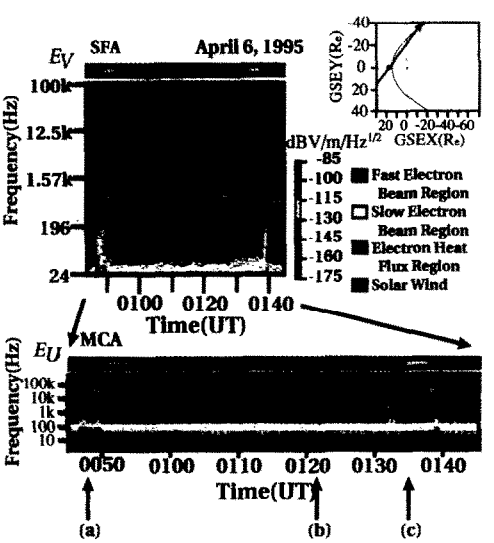

Fig. 3 Dynamic wave spectra observed in the electron foreshock. Upper and lower panels are generated from the SFA and MCA data, respectively. E_V and E_U denote each component of the orthogonal 2 electric field antennas, respectively. The white lines in each panel display the electron cyclotron frequency. Three different regions can be distinguished by different wave natures.

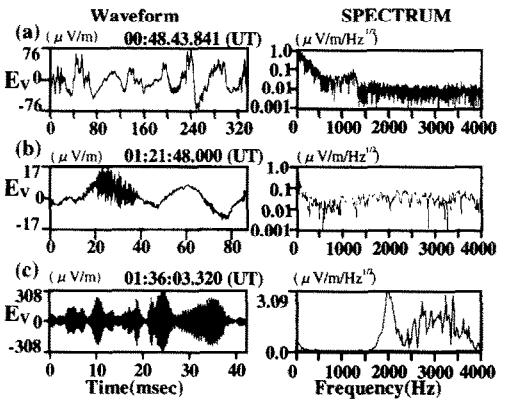

Fig. 5 Waveforms observed in (a) the fast electron beam region, (b) the electron heat flux region and (c) the slow electron beam region at different times indicated in Figure 3.

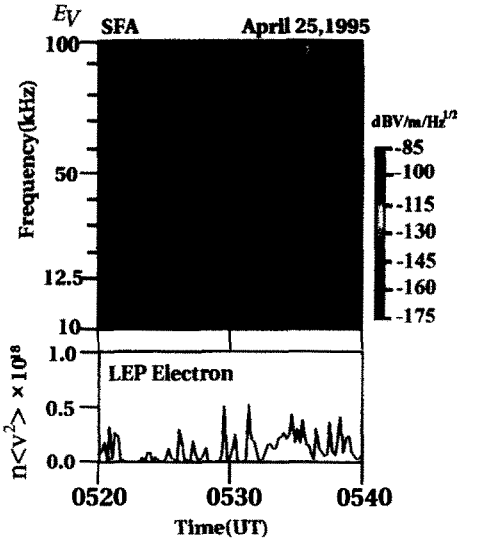

Fig. 4 Correlation of Langmuir waves near 23 kHz in the fast electron beam region with electron beam energy density. A good correlation between the two panels strongly suggests that the Langmuir waves are excited by the reflected electron beam from the bow shock.

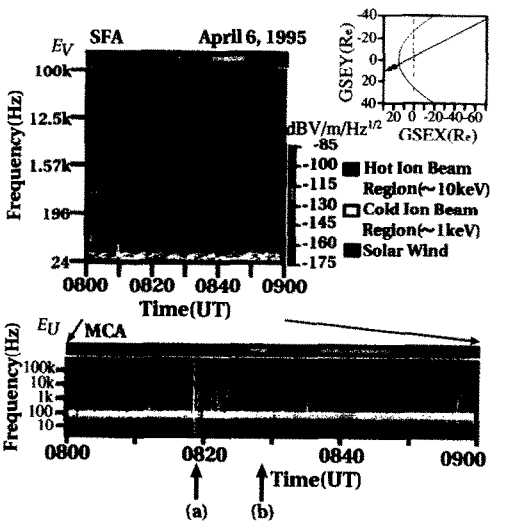

Fig. 6 Dynamic wave spectra observed in the ion foreshock. Two different regions can be distinguished by the difference of uppermost frequency of ion waves.

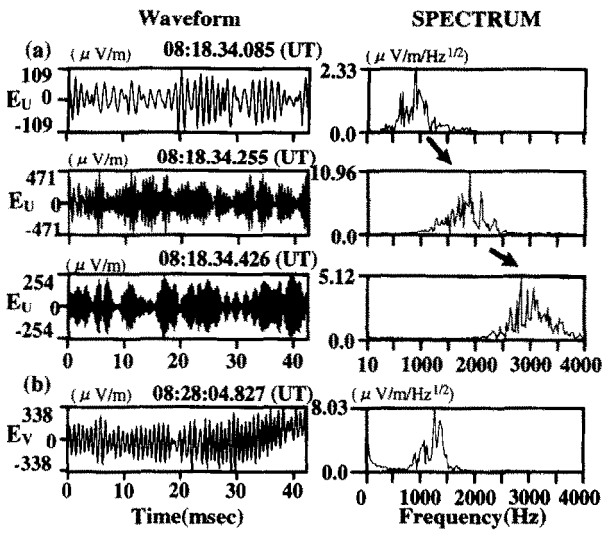

Fig. 7 Waveforms of ion waves (a) in the hot ion beam and (b) in the cold ion beam in the ion foreshock. The timing of the measurement is indicated by arrows in Figure 6.

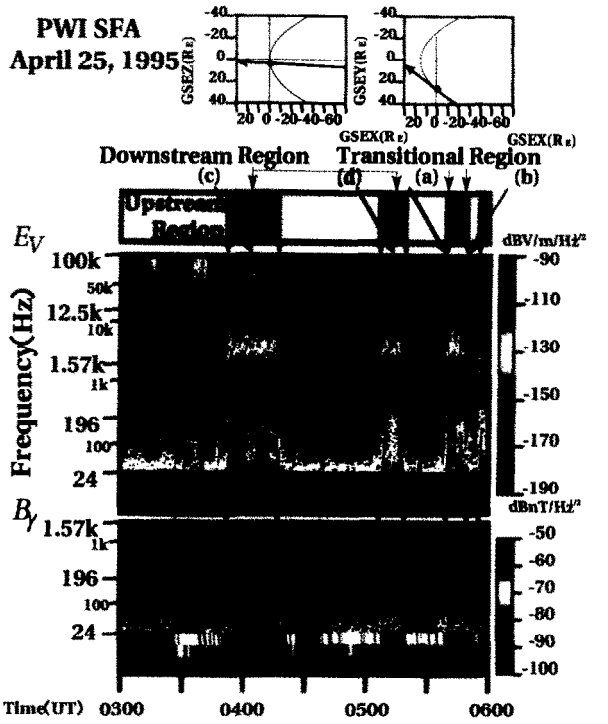

Fig. 8 Wave dynamic spectra by SFA at the multiple crossings of the bow shock on April 25, 1995. Abrupt enhancement of both E and B components at the crossings is seen over the broad frequency range.

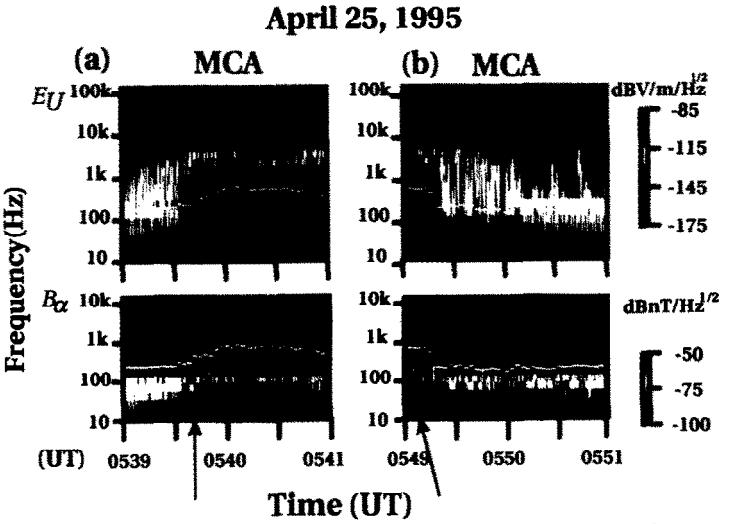

Fig. 9 Expanded wave spectra by MCA for 2 minutes at the entry and exit of the bow shock transition form and to the solar wind. The white lines indicate the electron cyclotron frequency.

SFA or MCA and could not identify their nature adequately. Computer simulations followed to understand the ESW in the plasma sheet boundary layer. They could well reveal a fact that a nonlinear BGK mode reached from an electron beam instability can well reproduce the characteristics of the observed ESW (Matsumoto *et al.*, 1994b; Omura *et al.*, 1994; Omura *et al.*, 1995)

In this paper, we describe preliminary results of our wave observation in the upstream region as well as in the shock transition and the downstream of the Earth's bow shock based on the SFA, MCA and WFC. The past observations (Greenstadt and Fredricks; 1979; Gurnett, 1985) have shown that the foreshock region can be divided into the electron and ion foreshocks based on the consideration of time-of-flight orbits of reflected electrons and ions form the bow shock. Gurnett (1985) discussed the wave features in the foreshock in detail and gave an overview of wave activities in the upstream and bow shock regions. He organized his discussion on waves in the foreshock distinguishing the electron and ion foreshocks. In the present paper we propose to classify the electron and ion foreshock regions further into sub-regions, respectively, based on the difference of the wave natures in each sub-regions. In the following sections, we show typical wave dynamic spectra in each sub-regions with their waveforms. Also described are the wave features in the shock transition regions and downstream of the bow shock in a similar format. Finally we briefly discuss possible interpretation of some of the waves observed in the upstream in terms of wave-particle interaction based on preliminary computer simulations.

PLASMA WAVES IN THE ELECTRON FORESHOCK

Figure 3 shows an example of plasma wave spectra in the electron foreshock on April 6 1995. The GEOTAIL location is depicted in the upper right corner by a dot. The arrow penetrating the dot shows the direction of the magnetic field at a time indicated in the frame. The upper left and lower frames show the dynamic spectra of electric field components (E_U and E_V) obtained by SFA and MCA, respectively (see Matsumoto *et al.* (1994a) for definition of E_U and E_V). The horizontal color bars above each frame indicate the region identification. The region identification is basically made by the difference of the wave natures with an assistance of the particle and magnetic field data. In the two time periods shown by the red mark around 0050UT and 0139, strong Langmuir waves (~25 kHz)are observed associated with enhanced low frequency waves below about 200 Hz. We call this region "fast electron beam region" as electron beams can run almost along the tangent field line which contacts the bow shock. Adjacent to this region, we see a region which is shown by the yellow bar called "slow electron beam region", where we see weaker Langmuir waves but do not see much wave activities below the electron plasma frequency. Further downstream adjacent to the slow electron beam is the region which we call "electron heat flux region" where we do not find well defined electron beam but a high energy tail with higher temperature. This region is characterized by weak Langmuir waves and simultaneous weak waves from below 10 Hz up to approximately 10 kHz.

It is established that the spectra of Langmuir waves in the electron foreshock is highly variable (Gurnett and Frank, 1975; Filbert and Kellogg, 1979; Anderson *et al.*, 1981; Gurnett, 1985). The upper panel of Figure 4 shows an expanded dynamic spectrum of Langmuir waves in the fast electron beam region of the electron foreshock. The Langmuir waves around 23 kHz are intensified intermittently. The lower panel shows the corresponding energy density of the electron beam component calculated from the GEOTAIL/LEP particle data. The peak in the beam kinetic energy density well correlates with the intensification of the Langmuir waves strongly indicating that the Langmuir waves are generated by the reflected electron beam from the bow shock.

Figure 5 shows the waveforms in three different subregions of the electron foreshock at three different times (a), (b) and (c) on April 6, 1996 which are indicated by arrows in Figure 3. In the fast electron beam region, the waveform in panel (a) shows that the low frequency part is mainly composed of waves with irregular waveforms in the frequency range of approximately 50 Hz. The spectral peak around 1.2 kHz

shown on the right panel is a result of the high frequency components superimposed on the lower frequency components in the waveform on the left. In the slow electron beam region as well as in the electron heat flux region, we see patchy dots in the SFA dynamic spectra in Figure 3 in the frequency range from 1 to 3 kHz. The corresponding waveforms are displayed in the panels (b) and (c). The panel (c) shows an example of fast variation in both frequency and amplitude of a quasi-monochromatic wave. The dynamic spectrum of this case (not shown) shows that the wave has a form of inverted hook in the frequency-time format. In the electron heat flux region, weak broadband noises background up to local electron plasma frequency are observed as seen in the SFA dynamic spectra in Figure 3. One example of the waveform corresponding to the weak broadband noises is shown in the panel (b). A bursty high frequency wave packet with a short duration of about 20 msec is superimposed on low frequency wave.

PLASMA WAVES IN THE IONS FORESHOCK

It is widely recognized that ion acoustic waves are often observed in the ion foreshock region (Scarf *et al.*, 1970; Anderson *et al.*, 1981; Rodriguez, 1981; Gurnett, 1985). Rodriguez (1981) suggests a possibility that these waves are not only the Doppler shifted ion acoustic waves but could be waves generated by Buneman instability due to slow electron beam. The GEOTAIL/LEP data (not shown) shows two distinct ion components are observed in turns during the passage in the ion foreshock region. One is filled with cold ions which temperatures are below several keV and the other is with hot ions above 10 keV. These cold and hot ions correspond to the "reflected" and "diffuse" ions defined in Gosling *et al.*(1978).

Figure 6 shows the wave dynamic spectra by SFA and MCA on April 6, 1996. The horizontal color bar in the top shows the regions of hot and cold ion beams in the ion foreshock based on the GEOTAIL/LEP data (not shown). In both regions, we can find very patchy red or yellow dots in the SFA plot. As the SFA sweeps the frequency slowly (64 sec for the lowest two bands, and 8 sec in the upper two bands in the figure), this shows that the spectrum of these waves varies in time very quickly. This can also be confirmed by the quick change of the frequency and intensity of the MCA plot in Figure 6. The difference between waves in the hot and cold ion regions is the uppermost frequency of these waves. In the hot ion beam region it reaches to approximately 10 kHz or more. In the cold ion beam region, it is below 1 kHz. The waveforms at different times (a) and (b) as indicated in Figure 6 which were chosen from the hot and cold ion beam regions, respectively are shown in Figure 7. The waveform sampled in the hot ion beam (the upper three panels) shows that the wave is a quasi-monochromatic wave with amplitude modulation and its central frequency rises with time. The frequency change in time is rapid, i.e., changes from about 700 Hz to 4 kHz in 0.35 sec. This rapid change in frequency has been pointed out by previous observation of ISEE-2 (Anderson *et al.*, 1981). The present observation has given its confirmation with additional information on waveforms. In contrast, the waves in the cold ion beam region, the frequency and amplitude are not much variable as shown by one example in panel (b) of Figure 7. The wave is quasi-monochromatic with rather constant frequency. It is surprising that the waves in the hot ion beam region consist of discrete riser elements. It may not be easy to understand their very fast frequency variation simply by Doppler shift of the ion acoustic waves as considered before.

PLASMA WAVES IN THE BOW SHOCK

Gurnett (1985) gave a good review on waves in the Earth's bow shock. He pointed out that the bow shock transition layer is characterized by an abrupt burst of electric and magnetic wave-field noise in association with the jump of magnetic field. Figure 8 shows an example of bow shock crossings met by GEOTAIL on April 25, 1995. During the time interval from 0300UT to 0600UT, GEOTAIL experienced the bow shock crossings 7 times. The three panels from the top show the location of the GEOTAIL, dynamic spectra of the electric components, and of magnetic components measured by SFA, respectively. It is evident that the electric wave field is suddenly enhanced at the crossing of the bow shock over a broad frequency range, from below 5 Hz to about 12 kHz. The wave intensity in the downstream of the transition region of

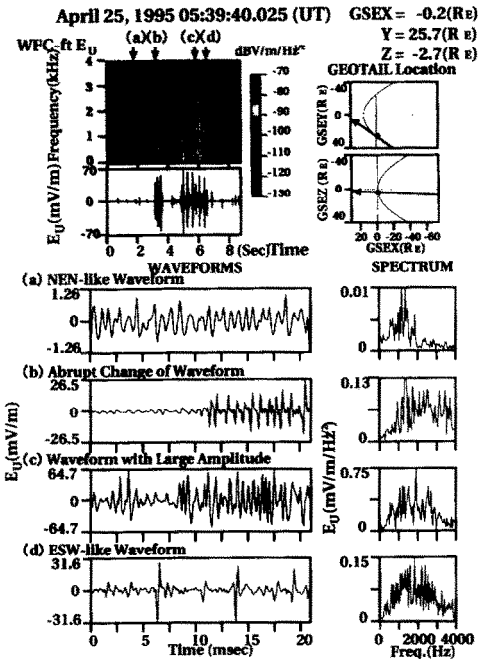

Fig. 10 Waveforms of plasma waves at the bow shock transition. The waves show highly variable intensities and waveforms within a very short time.

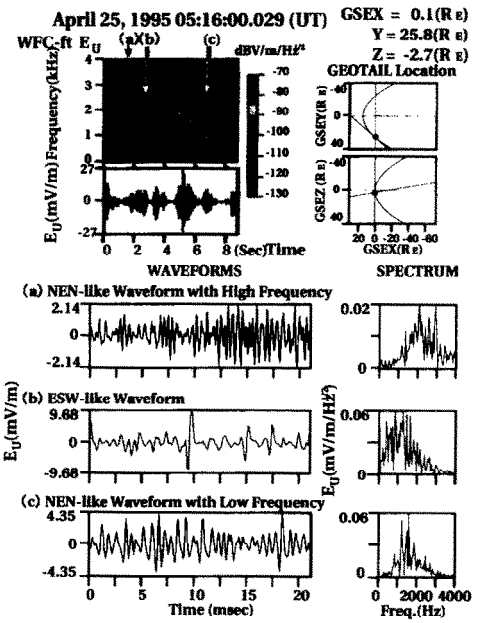

Fig. 11 Waveforms of plasma waves in the downstream of the bow shock.

Fig. 10 Waveforms of plasma waves at the bow shock transition. The waves show highly variable intensities and waveforms within a very short time.

Fig. 11 Waveforms of plasma waves in the downstream of the bow shock.

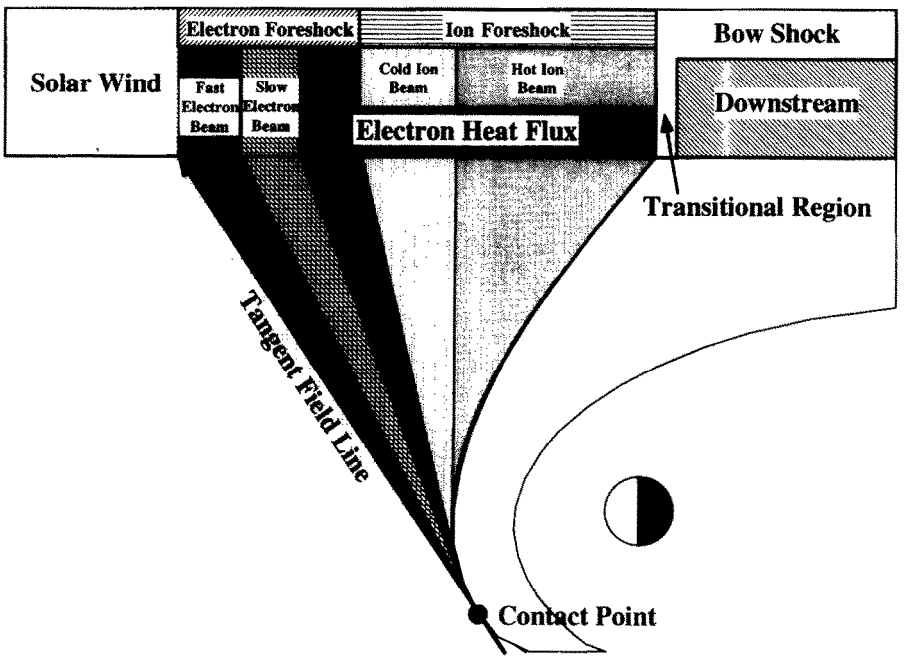

Fig. 12 Schematic drawing on the region divisions around the bow shock. Based on the plasma wave observations, we divided the electron and ion foreshocks into further 5 sub-regions.

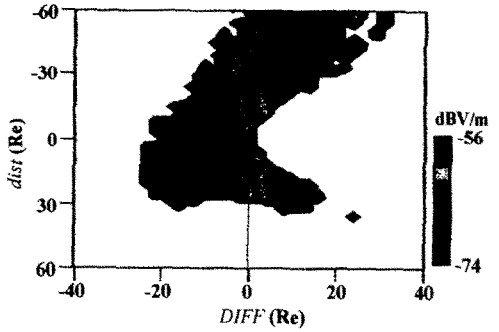

Fig. 13 Intensity mapping of Langmuir waves in the upstream based on the data from GEOTAIL/PWI.

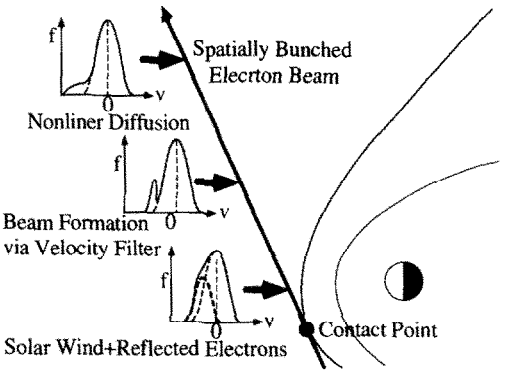

Fig. 14 A schematic illustration of beam formation and nonlinear diffusion along the tangent field line. Reflected electrons at the contact point forms a bump in the velocity space via velocity filter downstream along the field line. The formed beam hump is smoothed out via nonlinear wave-particle interaction.

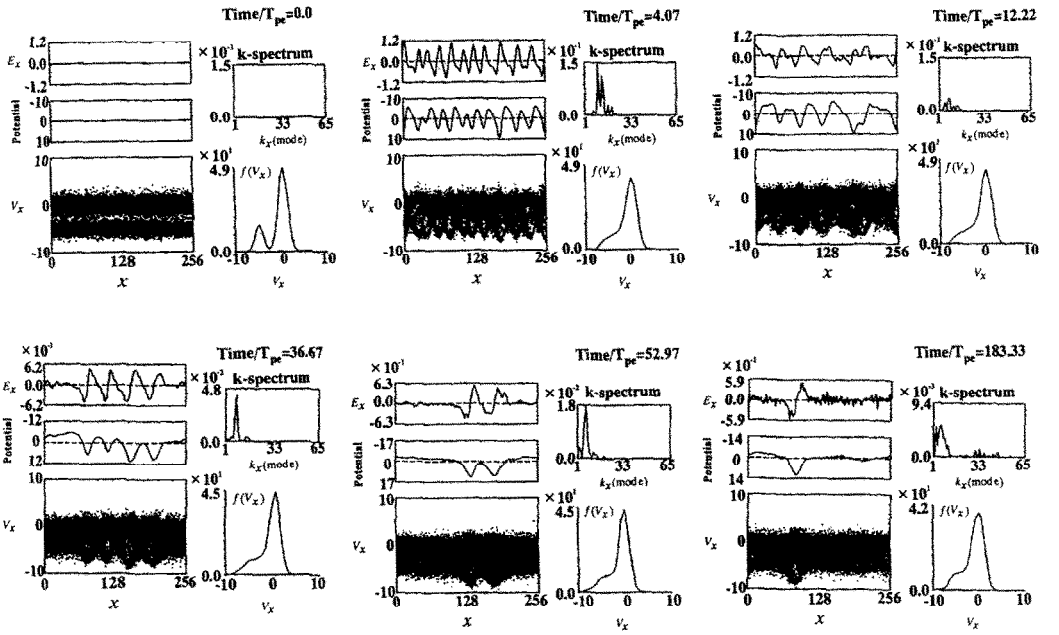

Fig. 15 Example of nonlinear evolution of bump-on-tail instability. Nonlinear trapping and succeeding further collapse of vortices destroy the hump and lead to the formation of plateau.

the bow shock is almost constant in the frequency range from about 200 Hz to 2 kHz, and is weakened with distance from the bow shock in the frequency range from 5 Hz to about 200 Hz. The magnetic field of the wave at the transition region extends from below 5 Hz to about the local electron cyclotron frequency which is shown by white dots in the SFA dynamic spectra. Behind the shock in the down stream, the maximum frequency of the magnetic components of the waves decreased down to several tens of Hz. The magnetic components represent whistler mode waves. We have examined the polarization of the whistler mode waves in the downstream of the shock and could verify the polarization of these bursty and whistler waves is right-handed. The relative intensity of the whistler waves reaches 10 to 20 % of the background geomagnetic field.

On this day, it was very fortunate that at the time marked by (a) in Figure 8, GEOTAIL could pick up the waveform data for 8.7 s at the transition region as it entered the bow shock from the upstream solar wind. At the time marked by (b) in the figure, GEOTAIL emerged from the shock into the solar wind. In the upstream Langmuir waves and 2fp emissions are clearly observed around 21kHz and 42 kHz, respectively. In much shorter time scale display the bow shock transition is more evident. Figure 9 shows the wave dynamic spectra by MCA for a period of two minutes near the times of (a) and (b) marked in Figure 8. The white lines indicate the local electron cyclotron frequency. The arrows below the horizontal axes of the MCA dynamic spectra show the timings of the WFC samplings. The first sampling at the time (a) was just on the ramp in the magnetic field in the midst of the bow shock transition region. The latter sampling at the time (b) was taken just inside the bow shock ramp behind the bow shock.

Though it is widely recognized the plasma waves in the transition region and downstream of the bow shock are highly turbulent and broadband (Gurnett, 1985), the plasma wave studies in this region have been based on the frequency spectra and not on the phase information. Figures 10 and 11 show the waveform data in the shock transition and the downstream the shock at the times (a) and (d) in Figure 8, respectively. In both figures, the two panels from the top shows the dynamic spectrum and waveforms in 8.7 sec. The lower four or three panels in Figure 10 and 11 show the waveforms at times indicated by arrows with labels (a), (b) etc. Two interesting features are read from the figures. One is a very rapid variation of the waveforms in a very short time. This is not surprising because the shock transition region passes the spacecraft very rapidly. However, it may be too simplistic to attribute the variability only to the fast motion of the shock. As seen in Figure 10, we have variety of waveforms: (a) quasi-monochromatic waveforms with relatively low intensity like NEN (Narrowband Electrostatic Noises) often observed near the boundaries such as PSBL and Magnetopause in the tail region, (b) an abrupt change from very quiet to nonlinear waveforms, (c) waves with very large amplitude but still remaining the characteristics of quasi-monochromaticity, and (d) a series of bi-polar pulses like BEN observed in the tail (Matsumoto *et al.*, 1994b). The corresponding frequency spectra are displayed on the right. It is evident that the spectral information alone could not tell the difference of the wave characteristics such as illustrated by the four waveforms which are completely different. In the downstream of the bow shock, the waveforms are more or less similar to those observed in the transition region. They are less intense as easily inferred from the consideration of the generation sources of these waves.

The information from WFC would be very helpful, if combined with computer simulations, in understanding wave-particle interactions in the shock transition region. Detailed analyses and related computer simulations are now under way and will be published in future.

DISCUSSION

The upstream and the bow shock are filled with interesting wave phenomena generated by microscopic wave-particle interactions. The inter-relation between macro- and micro- processes in these regions still remains uncertain partly because of the shortage of full understanding of the nature of the plasma waves. GEOTAIL added some useful information which may contribute to further understanding of the wave-

particle processes in these complicated region. As the present paper is based on the preliminary analyses of the GEOTAIL/PWI data, we have shown some of the interesting examples observed in these regions. Figure 12 schematically illustrates the characteristic regions which we proposed based on the plasma wave observations with an assistance of plasma and magnetic field measurements. As shown in this figure, we divide the electron and ion foreshock regions into further 5 sub-regions.

The electromagnetic waves, mostly whistler mode waves, have neither been included in the paper not because of their less importance, but simply because of the page limit. As to the Langmuir waves, we have made a statistical study by mapping their intensity in the *DIFF-dist* coordinates (e.g., see Figure9 in Filbert and Kellogg, 1979). Such mapping of Langmuir waves in the upstream have been attempted for the Earth (Greenstadt *et al.*, 1995) and for the Venus (Crawford *et al.*, 1993). The present study gives higher spatial resolution compared with the past contribution. Figure 13 shows the result of the mapping. The vertical axis, *dist*, is a distance from the contact point(CP) of the solar wind magnetic field line (called tangent field line) with the bow shock, and *DIFF* is the distance from the tangent field line to GEOTAIL location. It is clearly seen that the Langmuir activity near the CP (*dist* =0, *DIFF*=0). This means that the Langmuir waves are not generated near the CP on the tangent field line suggesting the reflected electrons do not form a bump on the tail in the velocity space near the CP due to the abundance of the population of the background population. This is schematically illustrated in Figure 14. However the Langmuir wave activity is enhanced beyond certain distance from the CP along the tangent field line. This can be explained by the velocity filter effect. Slower electrons in the reflected beam are swept downstream and thereby only the high speed component remain on or near the tangent field line producing a well-defined electron beam hump in the velocity distribution as illustrated in Figure 14. Further down along the tangent field line, the intensity of Langmuir waves decreases with increasing *dist*. Beyond 50 or 55 Re the Langmuir waves are no more observed. This may be due to nonlinear diffusion of the beam component in the velocity space. The nonlinear feedback to the velocity distribution due to the excited Langmuir waves destroys the hump and leads to the plateau formation in the velocity space as illustrated in Figure 14. Figure 15 is one example of such nonlinear process of collapse of the beam hump leading to the formation of the plateau. As time elapses, the initial electron beam excites the Langmuir wave. However soon after some time, the electrons are trapped by the potential well of the excited Langmuir wave creating vortices in the phase space. These vortices collide each other and merge each other reducing the number of vortex in the system. Detailed simulation of the nonlinear evolution of the beam-plasma system was published in Omura *et al.* (1995).

More work needs to be done on wave dynamics and related nonlinear dynamics in the upstream and bow shock regions, probably with a combination of data from the ISTP fleet and with efforts of computer simulations based on particle models.

ACKNOWLEDGMENTS

We thank S. Kokubun and T. Yamamoto for their GEOTAIL/MGF data, and D. Morikawa, S. Kudo, N. Miki, K. Ohtsuka for their help in data analysis. Discussions with Y. Omura and H. Usui on the result of the computer simulation and with appreciated. The simulation is carried out on the KDK system at RASC, Kyoto University. A part of this research has been supported by Grant-in Aid #08404027 by Monbusho.

REFERENCES

Anderson, R. R., G. K. Parks, T.E. Eastman, D. A. Gurnett, and L. A. Frank, Plasma waves associated with energetic particles streaming into the solar wind from the earth's bow shock, *J. Geophys. Res.*, 86 4493 (1981)

Crawford, G. K., R. J. Strangeway, and C. T. Russell, VLF imaging of the Venus foreshock, *Geophys. Res. Lett.*, 20, 2801 (1993).

Filbert, P. C., and P. J. Kellogg, Electrostatic noise at the plasma frequency beyond the bow shock, *J. Geophys. Res.*, 84, 1369 (1979)

Gosling, J. T., J. R. Asbridge, S. J. Bame, G. Pashman, and N. Sckopke, Observations of two distinct populations of bow shock ions in the upstream solar wind, *Geophys. Res. Lett.*, 5, 957 (1978).

Greenstadt E.W. and R. W. Fredricks, Shock systems in collisionless space plasmas, in *Solar System Plasma Physics, vol.3,* ed. by L. J. Lanzerotti, C. F. Kennel, and E. N. Parker, 3, North-Holland, Amsterdam (1979).

Greenstadt, E. W., G. K. Crawford, R. J. Strangeway, S. L. Moses, and F. V. Coroniti, Spatial distribution of electron plasma oscillations in the Earth's foreshock at ISEE3, *J. Geophys. Res.*, 100, 19933 (1995).

Gurnett, D. A. and L. A. Frank, Electron plasma oscillations associated with typeIII radio emissions and solar electrons, *Sol. Phys.*, 45, 477 (1975).

Gurnett, D. A., Plasma waves and instabilities, in *Collisionless shocks, Geophysical Monograph 35* ed. by B. T. Tsurutani and R. G. Stone, 207(1985).

Kojima, H., H. Matsumoto, T. Miyatake, I. Nagano, A. Fujita, L. A. Frank, T. Mukai, W. R. Paterson, Y. Saito, S. Machida, R. R. Anderson, Relation between electrostatic solitary waves and hot plasma flow in the plasma sheet boundary layer: GEOTAIL Observations, *Geophys. Res. Lett.*, 21, 2919 (1994).

Kojima, H., H. Hamada, H. Matsumoto, D. Morikawa, and R. R. Anderson, Statistical analyses of the plasma wave activities observed with GEOTAIL: Applications of plasma waves to the study of the geomagnetic structure, *to be submitted to J. Geophys. Res.*, (1997).

Omura Y., H. Kojima, and H. Matsumoto, Computer simulation of electrostatic solitary waves: A nonlinear model of broaddband electrostatic noise, *Geophys. Res., Lett.*, 21, 2923(1994).

Omura, Y., H. Matsumoto, T. Miyake, and H. Kojima, Electron beam instabilities as generation mechanism of electrostatic solitary waves in the magnetotail, *J. Geophys. Res.*, 101, 2685(1995).

Matsumoto, H., I. Nagano, R. R. Anderson, H. Kojima, K. Hashimoto, M. Tsutsui, T. Okada, I. Kimura, Y. Omura, and M. Okada, *J. Geomag. Geoelectr.*, 46, 59 (1994a).

Matsumoto, H., H. Kojima, T. Miyatake, Y. Omura, M. Okada, I. Nagano, and M. Tsutsui, Electrostatic solitary waves (ESW) in the magnetotail: BEN wave forms observed by Geotail, *Geophys. Res. Lett.*, 21, 2915 (1994b).

Rodriguez, P., Ion waves associated with solar and beam-plasma interaction, *J. Geophys. Res.*, 86, 1279 (1981).

Scarf, F. L., R. W. Fredricks, L. A. Frank, C. T. Russell, P. J. Coleman, Jr., and M. Neugebauer, Direct correlation of large amplitude waves with suprathermal protons in the upstream solar wind, *J. Geophys. Res.*, 75, 7316 (1970).